저작자표시-비영리-변경금지 2.0 대한민국

이용자는 아래의 조건을 따르는 경우에 한하여 자유롭게

- 이 저작물을 복제, 배포, 전송, 전시, 공연 및 방송할 수 있습니다.

다음과 같은 조건을 따라야 합니다:

저작자표시. 귀하는 원저작자를 표시하여야 합니다.

비영리. 귀하는 이 저작물을 영리 목적으로 이용할 수 없습니다.

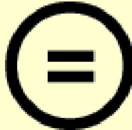
변경금지. 귀하는 이 저작물을 개작, 변형 또는 가공할 수 없습니다.

- 귀하는, 이 저작물의 재이용이나 배포의 경우, 이 저작물에 적용된 이용허락조건을 명확하게 나타내어야 합니다.
- 저작권자로부터 별도의 허가를 받으면 이러한 조건들은 적용되지 않습니다.

저작권법에 따른 이용자의 권리는 위의 내용에 의하여 영향을 받지 않습니다.

이것은 이용허락규약(Legal Code)을 이해하기 쉽게 요약한 것입니다.

Disclaimer

dCollection

이학석사 학위논문

Doping-Induced Optical and Electrical Properties of InSe FETs

2023 년 2 월

서울대학교 대학원

물 리 학 과

이 태 현

Doping-Induced Optical and Electrical Properties of InSe FETs

지도교수 이 지 은

이 논문을 이학석사 학위논문으로 제출함

2022 년 12 월

서울대학교 대학원

물 리 학 과

이 태 현

이태현의 이학석사 학위논문을 인준함

2023 년 2 월

위 원 장 ______ 김도헌 ______ (인)

부 위 원 장 ______ 이지은 ______ (인)

위 원 ______ 최현용 ______ (인)

Abstract

Doping-Induced Optical and Electrical Properties of InSe FETs

Taehyeon Lee
Department of Physics and Astronomy
The Graduate School
Seoul National University

Transition metal monochalcogenide is emerging as an interesting two-dimensional semiconductor in recent years. In particular, InSe has band structure strongly dependent on layer number with direct to indirect bandgap transition at 6-layer thickness. This induces exotic optical and electrical features which are actively being studied. With the help of external doping and intrinsic spin splitting, unique characteristics in doping dependent exciton emissons and electron spin textures can be detected. In this thesis, few-layer InSe field-effect transistors (FETs) were fabricated and the doping dependence of InSe's optical and electrical features is measured with photoluminescence spectroscopy and magneto-optical Kerr effect spectroscopy.

Keywords : InSe, doping, field-effect transistor, 2D materials, photoluminescence, spin texture
Student Number : 2020-27989

Table of contents

Abstract ··· i
Table of contents ··· ii
List of figures ··· iv

Chapter 1
Introduction ··· 1

Chapter 2
Background knowledge ··· 4
2.1 Two-dimensional (2D) materials ··· 4
2.1.1 Graphene ··· 6
2.1.2 Hexagonal boron nitride (hBN) ··· 7
2.2 Indium selenide (InSe) ··· 8
2.2.1 InSe's band characteristics ··· 9
2.2.2 Spin structure of InSe ··· 12
2.3 Many-body effect ··· 14

Chapter 3
Fabrication ··· 17
3.1 Device fabrication ··· 17
3.1.1 Device structure ··· 17

3.1.2 Graphene electrode ··· 19
3.1.3 InSe channel and hBN passivation ··· 20
3.1.4 HfO_2 substrate ··· 22
3.2 Device performances ··· 25

Chapter 4
Optical measurement ··· 27
4.1 Photoluminescence (PL) ··· 27
4.2 Magneto-optical Kerr effect (MOKE) ··· 29

Chapter 5
Results and discussion ··· 31
5.1 Doping-dependent photoluminescence of InSe ··· 31
5.1.1 Photoluminescence of InSe ··· 31
5.1.2 Doping dependence of trilayer InSe ··· 33
5.1.3 Doping dependence of six-layer InSe ··· 36
5.1.4 Discussion on the layer number dependence ··· 39
5.2 Preliminary data on spin measurement ··· 41
5.2.1 Spatial scan with zero bias voltage ··· 42
5.2.2 Spatial scan with non-zero bias voltage ··· 44

Chapter 6
Conclusion and future work ··· 47

References ··· 49

Abstract in Korean (국문 초록) ··· 53

List of figures

Figure 2.1 Schematic figure of 2D heterostructure consisting of hBN, InSe, and graphene. 5

Figure 2.2 **(a)** Top view of monolayer graphene. Solid black line is the unit cell. **(b)** Schematic band diagram of zero-doping, electron doping, and hole doping. 6

Figure 2.3 Top view of monolayer hBN. Solid black line is the unit cell. 7

Figure 2.4 **(a)** Side view of 4-layer γ-phase InSe **(b)** Top view of monolayer γ-phase InSe. Solid black line is the unit cell. Unit cell consists of trilayer InSe. 8

Figure 2.5 γ-phase InSe band structure of **(a)** monolayer, **(b)** trilayer, **(c)** five-layer, and **(d)** bulk. In the 2D limit, valence band shows Mexican hat shape indicating very low hole mobility. 9

Figure 2.6 Spin textures of monolyaer InSe for topmost valence band (left) and lowest conduction band (right) at the perpendicular electric field of 1.0 eV/Å. Color bar represents the out-of-plane component of spin quantization, while the arrows indicate the in-plane spin component. 13

Figure 2.7 Schematic figure of many-body effect. 14

Figure 3.1 Schematic figure of InSe field-effect transistor. The substrate is SiO_2 100 nm/Si. 17

Figure 3.2 Trilayer (left) and six-layer (right) sample on the SiO_2 substrate. The white scale bar corresponds to 15μm. Red, green, and blue dashed lines correspond to capping hBN, graphene electrode, and channel InSe, respectively. 18

Figure 3.3 Fabrication process of InSe FETs. InSe and hBN are directly exfoliated onto the PDMS/PPC film. 18

Figure 3.4 AFM profile. Degrading feature of γ-phase InSe in the ambient condition. After a day, γ-phase InSe changed to In_2O_3, and the thickness became more than double. 20

Figure 3.5 Schematic figure of InSe field-effect transistor. The substrate is HfO_2 30 nm/SiO_2 100 nm/Si. 22

Figure 3.6 Dielectric screening effect. The range of Coulomb potential induced by point charge defect is reduced. 24

Figure 3.7 The best device performances of **(a)** HfO_2 substrate sample and **(b)** SiO_2 substrate sample in the ambient condition. V_{sd} sweeps from $-10\,V$ to $+10\,V$ at $V_g = +10\,V$. The HfO_2 sample shows about 4 times improvement in current. 25

Figure 4.1 Photoluminescence spectroscopy setup (LP : linear polarizer, FM : flip mirror) ········ 27

Figure 4.2 Magneto-Optical Kerr Effect (MOKE) spectroscopy setup. (LP : linear polarizer, FM : flip mirror, FR : Fresnel rhomb, WP : Wollaton prism) ········ 29

Figure 5.1 PL spectrum of InSe (black) and fit function (blue). Green and red peaks correspond to defect-assisted recombination (peak 1) and direct electron-hole recombination (peak 2). ········ 31

Figure 5.2 Trilayer InSe photoluminescence measurement. **(a)** Raw data, **(b)** peak energy, **(c)** intensity, and **(d)** width. Peak 1 and peak 2 correspond to defect-assisted recombination and direct electron-hole recombination, respectively. ········ 33

Figure 5.3 Six-layer InSe photoluminescence measurement. **(a)** Raw data, **(b)** peak energy, **(c)** intensity, and **(d)** width. Peak 1 and peak 2 correspond to defect-assist recombination and direct electron-hole recombination, respectively. ········ 36

Figure 5.4 Schematic figure of defect generation in the few-layer γ-phase InSe. Se vacancies act as donors, which results in electron doping. ········ 39

Figure 5.5 (a) Optical image of the InSe sample. Blue, green, and red dotted line corresponds to InSe, graphene, and capping hBN, respectively. The white scale bar corresponds to 15μm. Spatial scan image of **(b)** reflection, **(c)** MOKE, and **(d)** current with zero bias voltage and $V_g = +20\,V$. Channel regions are indicated by green squares. The spin texture does not emerge when the bias current is zero. 42

Figure 5.6 Spatial scan image of **(a)** reflection, **(b)** current, and **(c)** MOKE with $V_b = +5\,V$ and $V_g = +20\,V$. Spatial scan image of **(d)** reflection, **(e)** current, and **(f)** MOKE with $V_b = -5\,V$ and $V_g = +20\,V$. Channel regions are indicated by green squares. 44

Chapter 1
Introduction

The mechanical exfoliation of an atomically thin graphene layer opened a new field of 2D materials [1]. Graphene's linear dispersion and massless Dirac Fermion are known to induce exotic phenomena which have been observed in many experiments [2,3].

Subsequently, transition metal dichalcogenides (TMDC) were revealed as new semiconductor members of 2D materials [4,5]. Monolayer TMDC such as MoS_2 and WSe_2 has a direct bandgap from near-infrared to visible range. Direct-to-indirect bandgap transition occurs above bilayer thickness, inducing contrasting optical responses. These band features attracted the attention of scientists in the related fields and a lot of research has been conducted on TMDC materials. For example, valley dependent phenomena [6-8] and spin-valley coupling effect [9] have been well-demonstrated.

Thanks to the discovery of various material groups and weak interlayer van der Waals coupling between individual layers, it is possible to create heterogeneous structures [10]. Through these heterostructures, the study of field-induced electrical properties of 2D

materials which requires elaborate device structures became possible. Nowadays, field-effect transistors [11] and dual-gated devices [12] are widely used device geometry of 2D materials.

When designing these electrical devices, the insulation layer is important. hBN has strong covalent bonding which is stable at high temperature and low density of charge-trapping defects [13]. Since hBN has a wide band gap (~6 eV) and atomically flat surface, it can be used as a substrate, a passivating layer, or an insulating layer.

Transition metal monochalcogenides (TMM) are another group of 2D semiconductor materials which have physical characteristics that are rarely seen in other 2D materials. Although some of TMM materials are known to have degradation feature in response to the ambient environment [14]. With the help of the above-mentioned advances in the fabrication processes, now TMM materials can be studied more systematically without degradation issue.

Recently, a member of TMM materials, γ-phase InSe is studied to reveal its unique physical properties. To list a few, bulk InSe is a direct gap semiconductor but shows a direct-to-indirect gap transition as the layer number decreases to monolayer, which is accompanied with varying excitonic emission properties. Also, the band structure of InSe shows a flat valence band in the 2D limit, which may induce very low hole mobility. Moreover, the inversion symmetry is broken in all layer number of the material, resulting in an inherent spin texture. With the passivation process to suppress degradation in ambient environment, device with a high electron mobility is

achievable which has been used to observe phenomena such as the quantum Hall effect [15].

In this thesis, photoluminescence (PL) and magneto-optical Kerr effect (MOKE) studies of InSe are reported. By inducing carrier doping in InSe transistors, we observed transition between excition and trion PL emission in InSe which shows different properties in tri-layer and six layer samples. By interpreting the observed data with existing theories, the unusual physical characteristics of the γ-phase InSe are identified. Also, preliminary data on MOKE measurements of InSe transistors shows possibilities of current-induced spin polarization with gate tunability.

Following the introduction, Chapter 2 presents background knowledge for the interpretation of InSe. After that, Chapter 3 covers the fabrication process in detail. Chapter 4 deals with hand-made optical measurement methods, including PL setup and MOKE setup. The most important part, Chapter 5, presents measurement data and discussions about results. Finally, the conclusions of the InSe study and its future work are presented in Chapter 6.

Chapter 2
Background knowledge

2.1 Two-dimensional (2D) materials

The two-dimensional (2D) material refers to a family of materials that bond between layers by weak van der Waals force. Graphene, hBN, transition metal dichalcogenide (TMDC), and transition metal monochalcogenide (TMM) are typical examples. Thanks to the weak interlayer coupling, this material family can be exfoliated into the 2D limit. Depending on the purpose of the experiment, the exfoliated flakes also can be combined to create heterostructures which show totally different physical features. These properties give physicists a rare opportunity to experimentally explore two-dimensional physics.

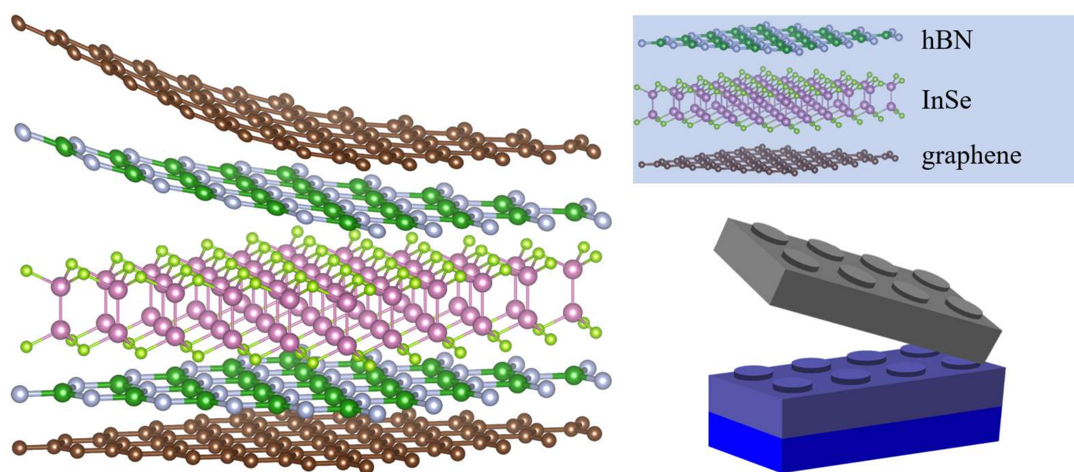

Figure 2.1 Schematic figure of 2D heterostructure consisting of hBN, InSe, and graphene.

2.1.1 Graphene

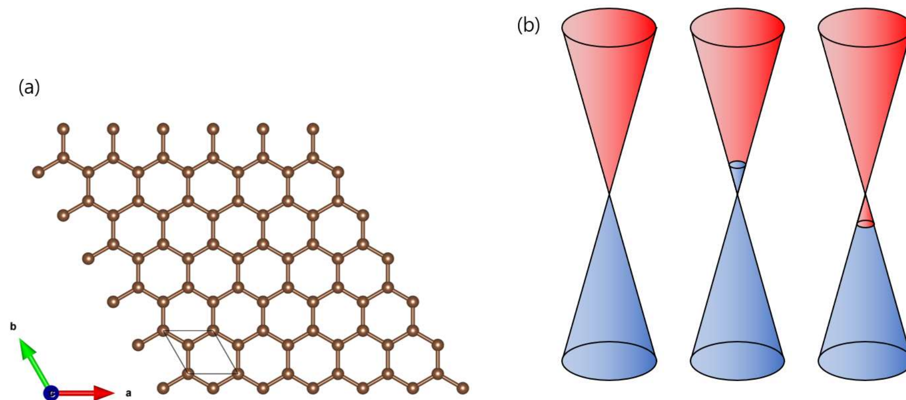

Figure 2.2 (a) Top view of monolayer graphene. Solid black line is the unit cell. **(b)** Schematic band diagram of zero-doping, electron doping, and hole doping.

Graphene, the first material that was successfully exfoliated in the 2D limit, has a hexagonal lattice structure composed of carbon atoms. Linear dispersion relation and massless Dirac Fermion are the key features that induce very high electron mobility and thermal conductivity. With the help of high tunability of work function by the gate voltage [16], it is widely used as a two-dimensional electronic device component. In addition, the 2D materials having atomic uniformity have better electrical contact with graphene than gold electrodes. Graphene flakes were used as an electrode in InSe field-effect transistor (FET) to obtain low contact resistance and ohmic contact with InSe.

2.1.2 Hexagonal boron nitride (hBN)

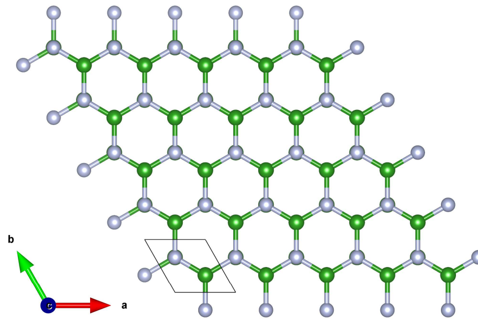

Figure 2.3 Top view of monolayer hBN. Solid black line is the unit cell.

A good quality insulating layer is essential when making electronic devices. High uniformity and low density of charge-trapping defects are necessary. The hBN, which has a hexagonal lattice structure consisting of covalent bonds between boron and nitrogen, is the member that meets these conditions. Having strong covalent bonding and a large insulating band gap, hBN prevents current flow through it and shows high thermal and electrical stability. As high-quality hBN with low density of charge-trapping defects became possible to produce [13], it is usually used as an atomically flat substrate or passivation layer. A few-layer hBN flake was used as a capping layer for all samples in this thesis.

2.2 Indium selenide (InSe)

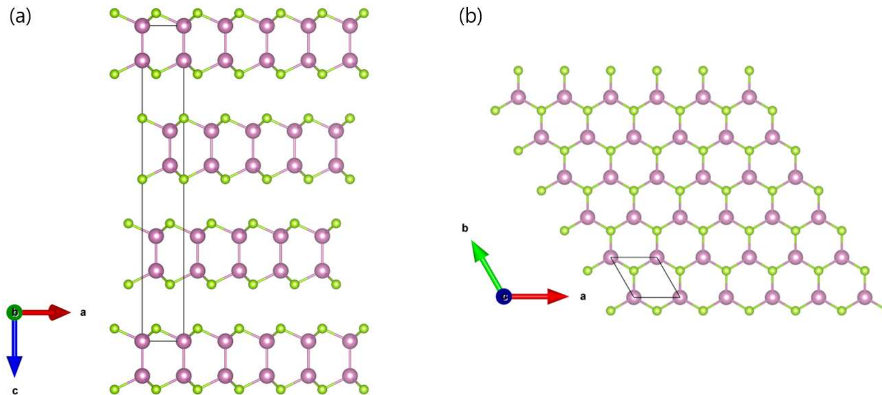

Figure 2.4 (a) Side view of 4-layer γ-phase InSe **(b)** Top view of monolayer γ-phase InSe. Solid black line is the unit cell. Unit cell consists of trilayer InSe.

InSe is a member of transition metal monochalcogenide (TMM). Recently, its high electron mobility and good optical response promoted optoelectronic research. Quantum Hall effect with high electron mobility of about 1000 cm^2/Vs in few-layer InSe at room temperature was reported [15]. There are also new optical properties [17] stemming from the lattice structure and band structure of InSe, which are completely different from other two-dimensional materials.

2.2.1 InSe's band characteristics

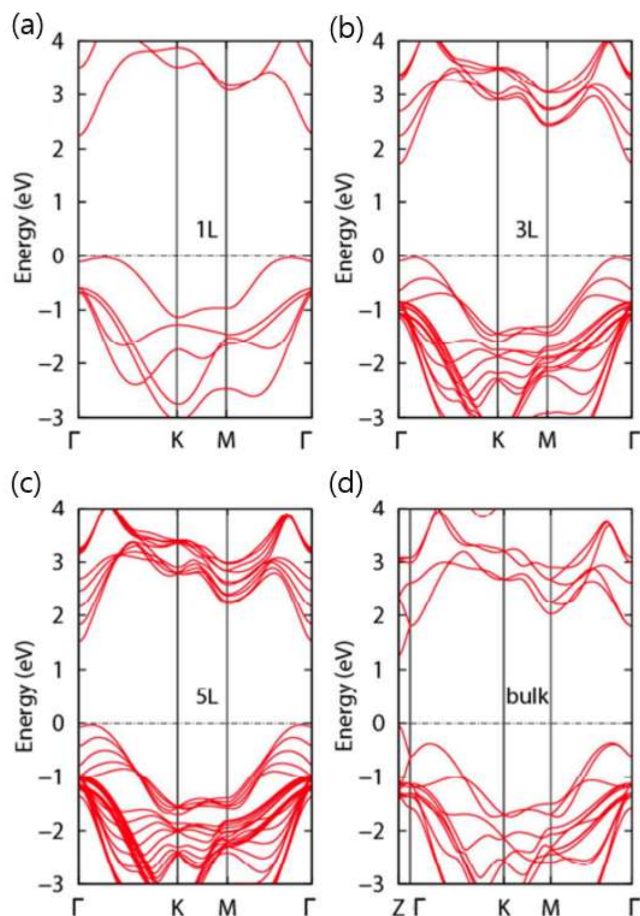

Figure 2.5 γ-phase InSe band structure of **(a)** monolayer, **(b)** trilayer, **(c)** five-layer, and **(d)** bulk. In the 2D limit, valence band shows Mexican hat shape indicating very low hole mobility. Reprinted with permission from Chaoyu Song, etal. *ACS Applied Materials & Interfaces 10* (4), 3994-4000 Copyright 2018 American Chemical Society.

The band structure of two-dimensional materials tends to be very dependent on the number of layers since there is a strong quantum confinement effect in the out-of-plane direction. Together with a large exciton Bohr radius stemming from low electron effective mass and high dielectric constant, the quantum confinement effect in InSe is stronger than TMDC [18]. As a result, the band structures of few-layer InSe are significantly changed by the layer number. These band features were verified either theoretically [19] or experimentally [15].

Especially, contrasting to the direct gap found in bulk InSe, when the number of layer goes down from seven to six, the valence band changes into a Mexican hat shape and the bandgap becomes indirect [19]. The origin of mexican hat-shaped valence band can be understood by the k • p theory. The hole mobility is given by the k • p theory as follows [20],

$$\frac{m_0}{m_n^*} = 1 + \frac{2}{m_0}\sum_{i \neq n} \frac{|\overleftrightarrow{p_{nj}}|^2}{E_n(\overrightarrow{k_0}) - E_j(\overrightarrow{k_0})}$$

where m_0 is the free-electron mass and $\overleftrightarrow{p_{nj}}$ is the momentum matrix element.

For InSe, the orbital composition of the conduction band minimum and valence band maximum is the s orbital of In and the p_z orbital

of Se. In this case, the momentum matrix element between the conduction band minimum and the valence band maximum is vanished by the selection rule. In addition, since the second and third valence bands are very close, the negative terms become very large. As a result, hole mobility became negative at the gamma point. As momentum is away from the gamma point, p_x and p_y orbital components of Se emerge. These components make the momentum matrix element between the conduction band minimum and the valence band maximum not vanished. Consequently, the hole mobility value gradually obtains a positive value, which results in Mexican hat shaped-valence band.

At this point, what should be emphasized is the flatness of the valence band, which means extremely low hole mobility. These characteristics which have not been seen in the previous two-dimensional materials induce a very unusual tendency in the optical and electrical responses.

2.2.2 Spin structure of InSe

As it can be seen in the lattice structure, except monolayer's mirror symmetry along the c-axis, γ-phase TMM materials including InSe have broken inversion symmetry. For broken inversion symmetry with external gate voltage applied, two types of spin-orbit interactions (SOI) play a crucial role in the spin interaction. One is the Dresselhaus spin-orbit coupling (SOC) stemming from crystal structure asymmetry. So the Dresselhaus SOC is inherent in the lattice structure. And the other is the Rashba SOC induced by the potential energy asymmetry of the electron system. Therefore, Rashba SOC can be manipulated easily by the external electric field. Each term can be calculated by the first principle method.

First-principle study on the spin texture of InSe indicate that the spin Hall conductivity exists and can be very strong when the two factors are coupled [21]. As a result of the coupling, the energy band of the InSe splits depending on the spin direction. The spin texture for monolayer InSe is given in Figure 2.6. The spin is locked to their momentum within their subband. Coupling with high mobility, spin current can be generated to the point where it can be measured optically.

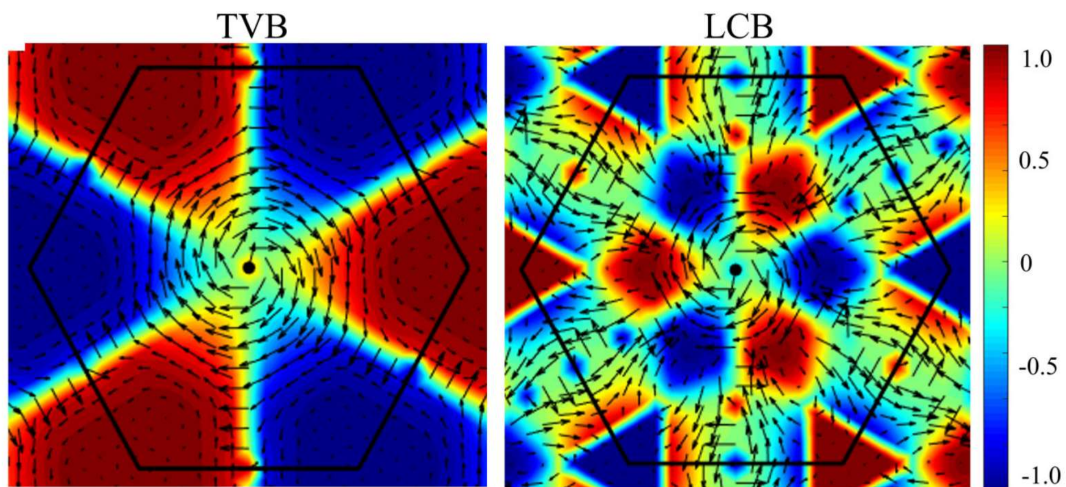

Figure 2.6 Spin textures of monolyaer InSe for topmost valence band (left) and lowest conduction band (right) at the perpendicular electric field of 1.0 eV/Å. Color bar represents the out-of-plane component of spin quantization, while the arrows indicate the in-plane spin component. Reprinted with permission from Farooq, M. Umar, et al. *Physical Review B* 105.24 245405. Copyright 2022 American Physics Society.

2.2.3 Many-body effect

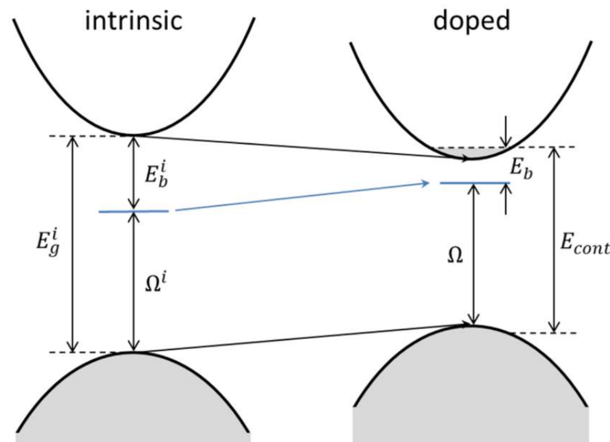

Figure 2.7 Schematic figure of many-body effect. Reprinted with permission from Gao, Shiyuan, et al. *Nano letters* 16.9 5568-5573. Copyright 2016 American Chemical Society.

In this section, to give a background on the analysis given in Chapter 5 on doping dependent photoluminescence data of InSe, Pauli blocking effect and many-body effects that needs to be considered when interpreting exciton emission are presented.

Photoluminescence is the result of all radiative recombination. Therefore, To analytically address the photoluminescence signal, one should consider all possible perturbations affecting band structure or electrical potential in the system. Since this is the problem with complex many-body electron systems with various perturbations, these

effects are called many-body effects. Especially, 2D materials have strong many-body interactions due to the enhanced quantum confinement effect. In the case of field-effect transistors, These interactions are divided into four components: Pauli blocking, Elastic Coulomb scattering, band gap renormalization, and reduction of exciton binding energy.

Pauli blocking is a phenomenon that results from the Fermionic nature of electrons. When the gate voltage makes the system doped with electrons, some parts of states around the conduction band are now forbidden from exciton formation as demonstrated in the Figure 2.7 [22]. This effect increases the photoluminescence energy and the band geometry determines how much it increases.

Elastic Coulomb scattering is the scattering process where excitons scatter with excessive free charge carriers induced by electrical doping. This scattering decrease the exciton coherency. Combined with the quantum confinement effect, the photoluminescence signal's broadness increases. The extent of the broadness is determined by the free charge carrier's effective mass and concentration [23].

Band gap renormalization comes from the screening effect. Excessive charges screen the whole system's Coulomb potential. Since this screening effect modifies the 'cloud' which comes from surrounding particles such as electrons, holes, excitons, and phonons, the overall change in the effective Hamiltonian occurs. So, the resultant change in physical variables is 'renormalized' rather than 'corrected' or 'changed' like electron mobility. This overall reduction in electrical Coulomb

potential leads to the renormalization of the band strcuture. Previously, an angle-resolved photoemission spectroscopy (ARPES) measurement of InSe demonstrated the decrease in photoluminescence energy about 120 meV as a function of electron concentration [24].

Reduction in exciton binding energy also stems from the screening effect. Reduced attractive force by screening effect decreases the exciton binding energy. This increases the photoluminescence energy [25].

Also, in addition to exciton, in the mild electron doping regime, the negative trions emerge. As a recombination process, trions can dissociate while emitting photons. Unlike the exciton, a negative trion leaves one electron after the dissociation process. Therefore, the Fermi energy increased by electron doping should also be added to trion dissociation energy. This results in the red-shift of the photoluminescence energy when trion emssion is associated [25].

Besides gate-induced doping, another factor should also be considered. A free charge carrier is created not only by gating but also by laser excitation. These laser-induced free charge carriers have same roles. These electro-optical factors come together to influence how the photoluminescence signal of InSe changes [26].

Chapter 3
Fabrication

3.1 Device fabrication

3.1.1 Device structure

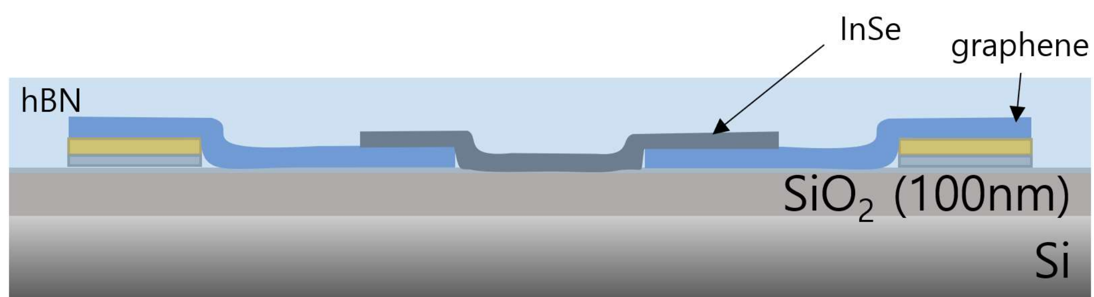

Figure 3.1 Schematic figure of InSe field-effect transistor. The substrate is SiO_2 100 nm/Si.

As illustrated in Figure 3.1, the InSe field-effect transistor was fabricated on a pre-patterned gold electrode on a SiO2 100 nm/Si substrate. The graphene flakes were transferred onto the gold

electrode. InSe and hBN were transferred sequentially between the graphene electrodes. and on top of the whole sample, respectively.

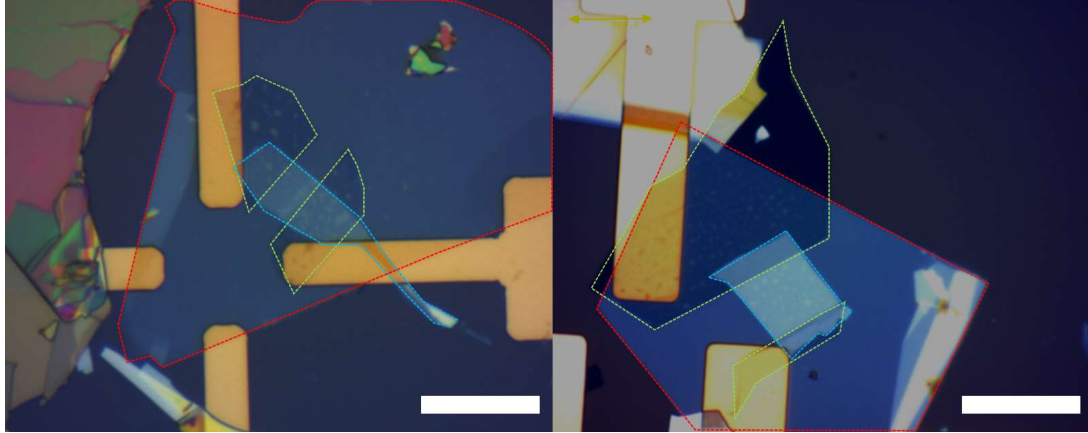

Figure 3.2 Trilayer (left) and six-layer (right) sample on the SiO_2 substrate. The white scale bar corresponds to 15μm. Red, green, and blue dashed lines correspond to capping hBN, graphene electrode, and channel InSe, respectively.

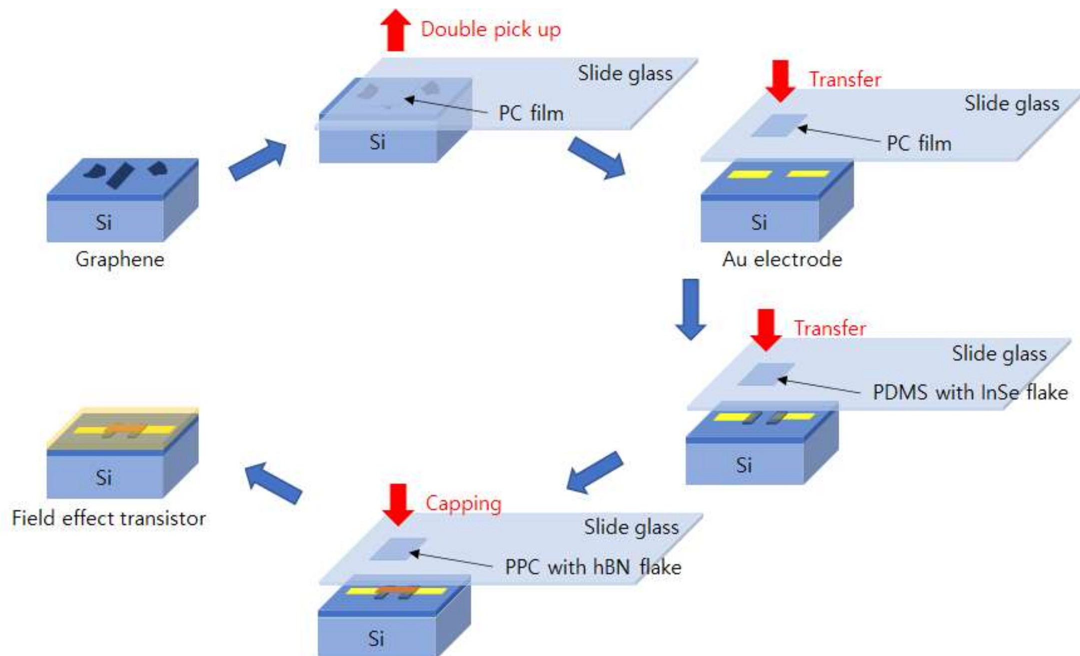

Figure 3.3 Fabrication process of InSe FETs. InSe and hBN are directly exfoliated onto the PDMS/PPC film.

3.1.2 Graphene electrode

After testing the graphite mother bulk by room temperature probe station, Graphene flakes were exfoliated onto SiO_2 100 nm/Si substrate on ambient condition. Using polycarbonate (PC) film (PC 6%/Chloroform) and dry transfer technique, graphene flakes were transferred onto a pre-patterned Au electrode. Cleaning with Chloroform 30 mins/Acetone 10 mins/IPA 10 mins was done after transfer. To remove bubbles and any residue on the graphene surface and electrode/graphene interface, 200 ˚C 2 hrs vacuum ($< 1.0 \times 10^{-3}\, torr$) annealing was carried out in the tube furnace. This process also reduced the contact resistance by making the graphene clean and adhere to the Au electrode well.

3.1.3 InSe channel and hBN passivation

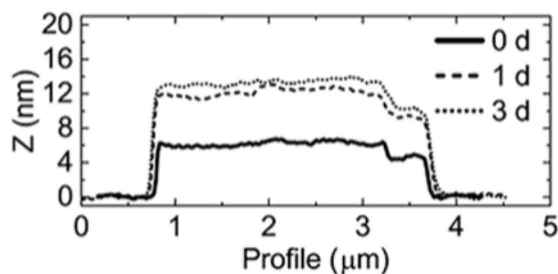

Figure 3.4 AFM profile. Degrading feature of γ-phase InSe in the ambient condition. After a day, γ-phase InSe changed to In_2O_3, and the thickness became more than double. Reprinted with permission from Wells, S. A,etal. NanoLett. 18, 7876 - 7882 Copyright 2018 American Chemical Society.

Since InSe shows strong degrading features under ambient condition, InSe flakes were exfoliated onto the PDMS substrate in the glove box(< $5.0 ppm$ for O_2 and H_2O). As a channel material for the field-effect transistor, InSe flakes were directly transferred onto the graphene electrode in the glove box. To prevent potential degradation during measurement, capping is crucial for study of air degrading materials. At the same time, to conduct an optical experiment, the capping layer's absorption should be low. So, few-layer hBN flake

was used as a capping layer. Polypropylene carbonate (PPC) film (PPC 12%/Anisole) was prepared by baking 10 mins at 120 ˚C on a hotplate. Few-layer hBN was directly exfoliated onto PPC film (PPC 12%/Anisole). Lastly, in the glove box, few-layer hBN was transferred onto the whole region(graphene, InSe, graphene/Au interfaces) to press all flakes together. In this way, contact resistances at the interfaces could be reduced.

3.1.4 HfO_2 substrate

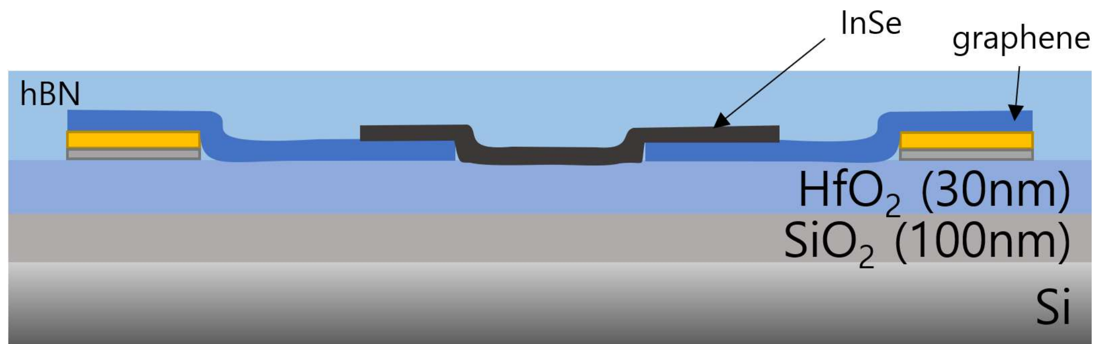

Figure 3.5 Schematic figure of InSe field-effect transistor. The substrate is HfO_2 30 nm/SiO_2 100 nm/Si.

Many defects are distributed near the surface. The two-dimensional materials have a large proportion of the near-surface volume to the total volume. So physical properties of two-dimensional materials are greatly affected by defects [27]. This high density of intrinsic defects increases charge-defect scattering, affecting overall physical properties including photoluminescence spectrum, bias current level, and unintentional doping.

Another factor that greatly influences two-dimensional electronic devices is the charge-trapping defects and non-atomically flat surface of the traditional substrate such as the SiO_2 substrate [28]. Due to the high density and randomness of the charge-trapping defects in SiO_2

substrate, early field-effect transistors consisting of a TMDC showed both n-type [4] and p-type [29] behavior depending on substrate.

The dielectric screening is a promising technique to remove the above-mentioned defect effects. Dielectric mismatching at the channel/environment interface modifies the Coulomb potentials inside an ultra-thin semiconductor layer [30]. For a theoretical calculation example, the channel dielectric constant $\epsilon_s = 7.6$ with environment dielectric constant $\epsilon_e = 1, 7.6 (= \epsilon_s), 100$ case is shown in Figure 3.6. The range of the calculated Coulomb potential induced by charge defect is significantly reduced, making the unintentional scattering almost diminished. At the same time, the electric field flux leakage toward the environment also decreases. This technology, which has been experimentally and theoretically verified, is widely used in this field now.

Since HfO_2 has a high dielectric constant and can be deposited by atomic layer deposition with atomic uniformity, HfO_2 was used as the dielectric screening substrate in some devices fabricated in this work. HfO_2 30 nm was deposited by an atomic layer deposition system (LUCIDA D100). Photolithography was carried out using DL-1000A1 maskless aligner and e-beam evaporator was used to deposit electrode with Ti 5 nm/Au 25 nm. Afterward, all fabrication process was the same with SiO_2 devices.

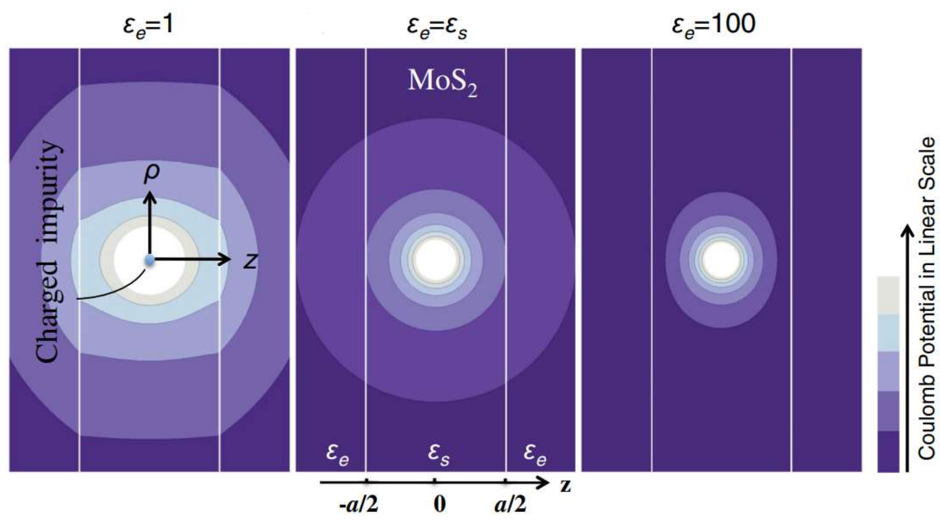

Figure 3.6 Dielectric screening effect. The range of Coulomb potential induced by point charge defect is reduced. Reprinted with permission from Ma, N, et al. Phys. Rev. X4, 011043 Copyright 2014 American Physics Society.

3.2 Device performances

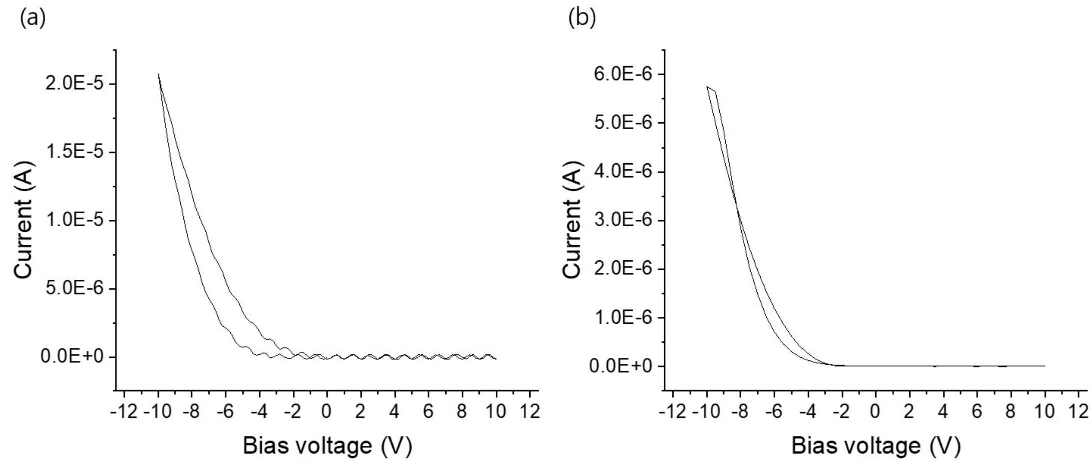

Figure 3.7 The best device performances of **(a)** HfO_2 substrate sample and **(b)** SiO_2 substrate sample in the ambient condition. V_{sd} sweeps from $-10\,V$ to $+10\,V$ at $V_g = +10\,V$. The HfO_2 sample shows about 4 times improvement in current.

In the SiO_2 samples, the electron mobility varied significantly for each device. The lowest was 0.2 cm^2/Vs, and the highest was 240 cm^2/Vs in the ambient condition. During the fabrication process, invisible cracks, ripples, and bubbles could occur. High contact resistance stemming from rough surfaces, vacuum gaps, and remaining residue also could exist. These factors influence the conductivity of InSe FETs. For the best case of the SiO_2 sample, bias current flowed about $5.7\mu A$ at $V_g = +10\,V$. With this order of bias

current, the spin texture is possible for detection by magneto-optical Kerr effect (MOKE) spectroscopy.

Applying the dielectric screening technique with HfO_2, two HfO_2 samples were made. For the best case, the bias current flowed $22\mu A$ at $V_g = +10\,V$, which means about four times enhancement compared to SiO_2 substrate. At room temperature, the channel current is dominated by phonon scattering, so it is also expected that the channel current would be improved by effects other than the dielectric screening effect. The most possible origin is the atomic flatness of HfO_2 substrate. With more samples and fabrication optimization, it will become possible to get higher order of bias current at low temperature.

Chapter 4
Optical measurement

4.1 Photoluminescence (PL)

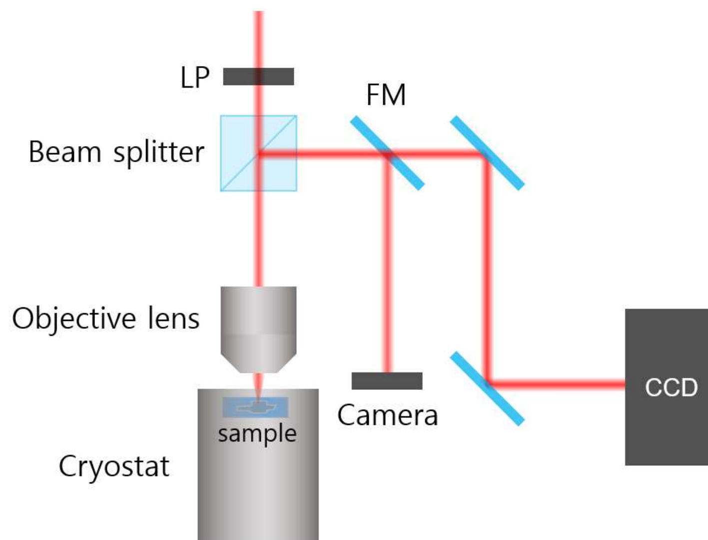

Figure 4.1 Photoluminescence spectroscopy setup (LP : linear polarizer, FM : flip mirror)

An excitation laser with 532 nm laser wavelength was used with 96 μW intensity. The reflected signal from the sample was collected with an objective lens and entered into the charge-coupled device (CCD).

The band gap of InSe changes rapidly depending on the number of layer. Therefore, the PL peak position also changes very significantly. So the layer number could be determined from PL peak position.

After the identification of layer number, doping dependence of photoluminescence was measured with InSe FETs. Since few-layer InSe shows exotic band structure which is characterized by the Mexican hat shape, the collected photoluminescence signal's tendency is also expected to be unusual. While measurement was conducted, channel InSe was grounded and the gate voltage was applied to the backside Si by the data acquisition (DAQ) board.

Another purpose of PL measurement is to determine the optimized wavelength for Kerr rotation measurement because maximum absorption tends to occur in the middle of the right shoulder of the photoluminescence peak in the energy scale. It is essential to satisfy this wavelength condition because direct observation of the intrinsic spin textures by optical measurement requires strict optimization.

4.2 Magneto-optical Kerr effect (MOKE)

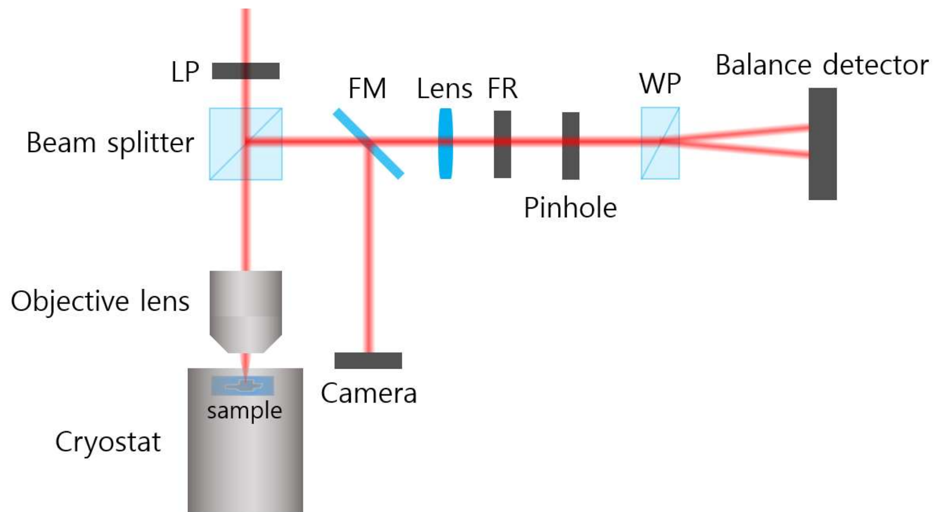

Figure 4.2 Magneto-optical Kerr effect (MOKE) spectroscopy setup. (LP : linear polarizer, FM : flip mirror, FR : Fresnel rhomb, WP : Wollaton prism)

The used probe laser source was a linearly polarized diode laser. The optimized wavelength for the probe laser was chosen from the photoluminescence measurement. If the probed region of the sample has net magnetization, then the reflected laser probe's polarization rotates with some angle which is called Kerr rotation. With the normal incidence of probe laser, polarization rotation comes from the out-of-plane net magnetization. Also, Since InSe does not have long-range magnetic ordering, the measured MOKE signal is

originated from the out-of-plane current-induced spin polarization. Fresnel rhomb and Wollaston prism resolve the rotation angle and the balance detector read it.

The goal of Kerr rotation measurement is to optically detect the spin phenomena caused by bias current when field-effect doping is applied. So, to read Kerr rotation, reflection, and current at the same time, three lock-in amplifiers (SR-830) were used. One of the lock-in amplifiers applies AC voltage into the source electrode of InSe channel by its own internal function generator to induce sinusoidally varying bias current. The applied AC voltage's frequency was locked into two lock-in amplifiers so that frequency modulated signals of Kerr rotation and current can be detected with low noise. One of the lock-in amplifier is connected to optical chopper in the laser path for detecting reflection. Lastly, the gate voltage to the InSe channel to increase the doping level was applied by DAQ board.

Chapter 5
Results and discussion

5.1 Doping-dependent photoluminescence of InSe

5.1.1 Photoluminescence of InSe

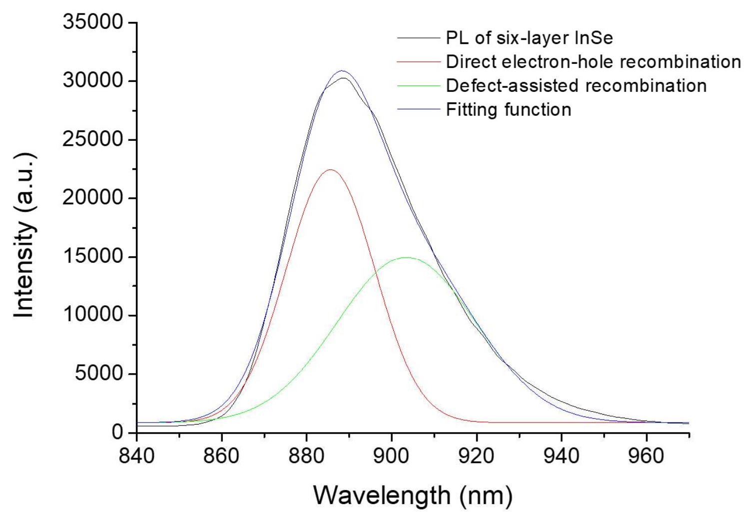

Figure 5.1 PL spectrum of InSe (black) and fit function (blue). Green and red peaks correspond to defect-assisted recombination (peak 1) and direct electron-hole recombination (peak 2).

Figure 5.1 shows the photoluminescence of six-layer InSe measured at 5.6 K with the laser power of 96 μW. The black line shows the measured data and it can be well fitted using the addition of two Gaussian functions which is indicated by the blue line. The origin of the two Gaussian fit functions are explained below.

At low temperature, InSe's photoluminescence has two main components. One is a defect-assisted recombination component with lower energy and the other is a direct electron-hole recombination component with higher energy. Previous time-resolved photoluminescence study on InSe demonstrated these components [31]. Due to two peak components with different energies, asymmetric photoluminescence signals were observed for every InSe FETs. So all photoluminescence data is fit by two components as in Figure 5.1. The layer number was configured by the higher energy component which corresponds to direct band-to-band electron-hole recombination.

5.1.2 Doping dependence of trilayer InSe

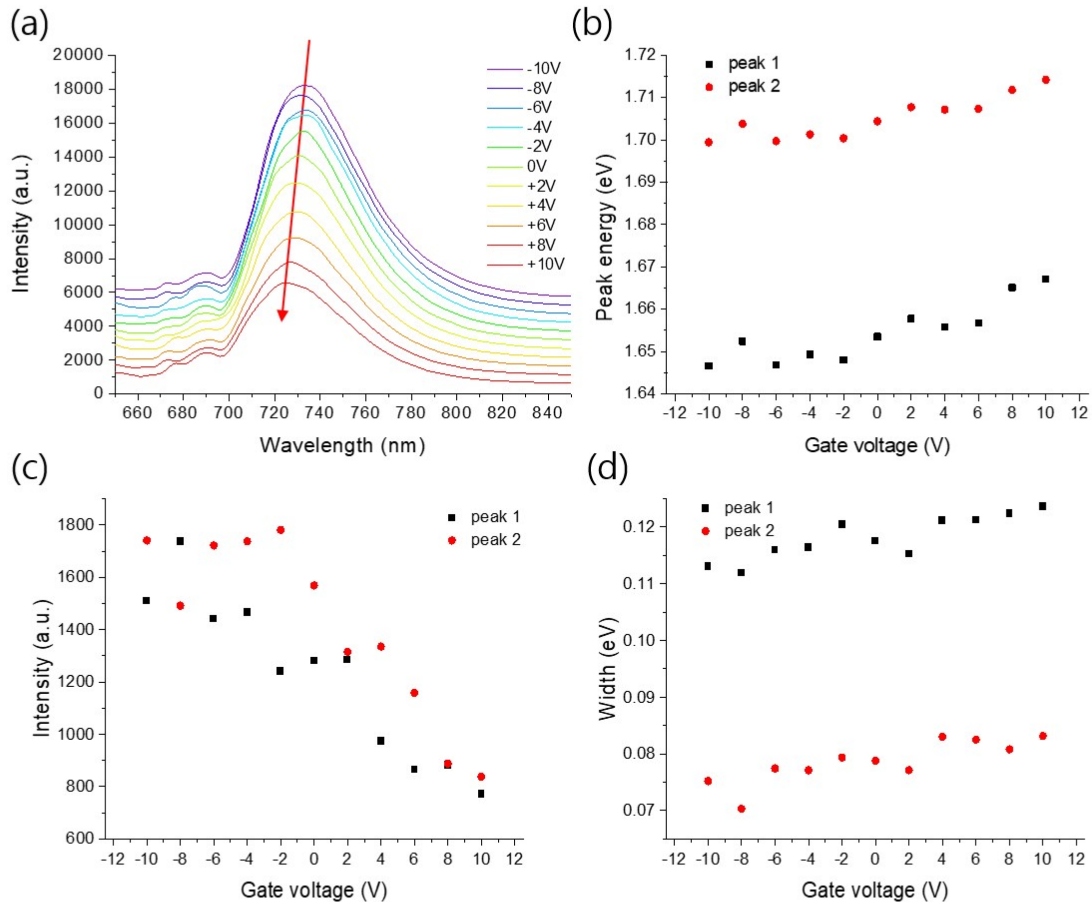

Figure 5.2 Trilayer InSe photoluminescence measurement. **(a)** Raw data, **(b)** peak energy, **(c)** intensity, and **(d)** width. Peak 1 and peak 2 correspond to defect-assisted recombination and direct electron-hole recombination, respectively.

Trilayer sample shows a monotonous tendency of decreasing intensity, increasing energy, and increasing width as the gate voltage increased from $-10\,V$ to $+10\,V$. Due to a very large difference between hole mobility and electron mobility at this layer number, the PL tendency would rapidly change when passing through the charge neutral point. However, since we did not observe sudden change of PL emission properties within the measurement range, the trilayer sample has no charge neutral point in the gate voltage range from $-10\,V$ to $+10\,V$.

Because the measurement was conducted at 5.6K, changes in the charge concentration due to applied gate voltage cause activation of other quasi-particles. The most likely quasi-particles are trion and biexciton. In the mild doping regime, the mainly induced quasi-particle is the trion. However, our measurement result shows that exciton emission is the main emission source for tri-layer sample in all voltage range rather than trion due to the following reason.

The observed PL intensity would show a local maximum at the charge neutral point which is expected to be at negative voltage further below the measurement range, so trilayer sample operates in the mild electron doping regime. Since negative trions show a tendency to redshift as the electron concentration increase in contrast to our data, the radiative recombination in the measurement voltage region is dominated by excitons which show a tendency of mild

blue-shift (~10 eV) instead of trion. This blueshift has a similar value to the previously studied TMDC material group [23,25]. The origin of the PL emission blue shift with increasing electron concentration is that the blue shift due to exciton binding energy and Pauli blocking is larger than the red shift from bandgap renormalization.

Lastly, the width increases due to increased elastic Coulomb scattering between excessive electrons and excitons. As the gate voltage increases, the concentration of electrons also increases, which increase the scattering rate. This makes exciton emission to be incoherent, inducing an increase in photoluminescence width.

5.1.3 Doping depedence of six-layer InSe

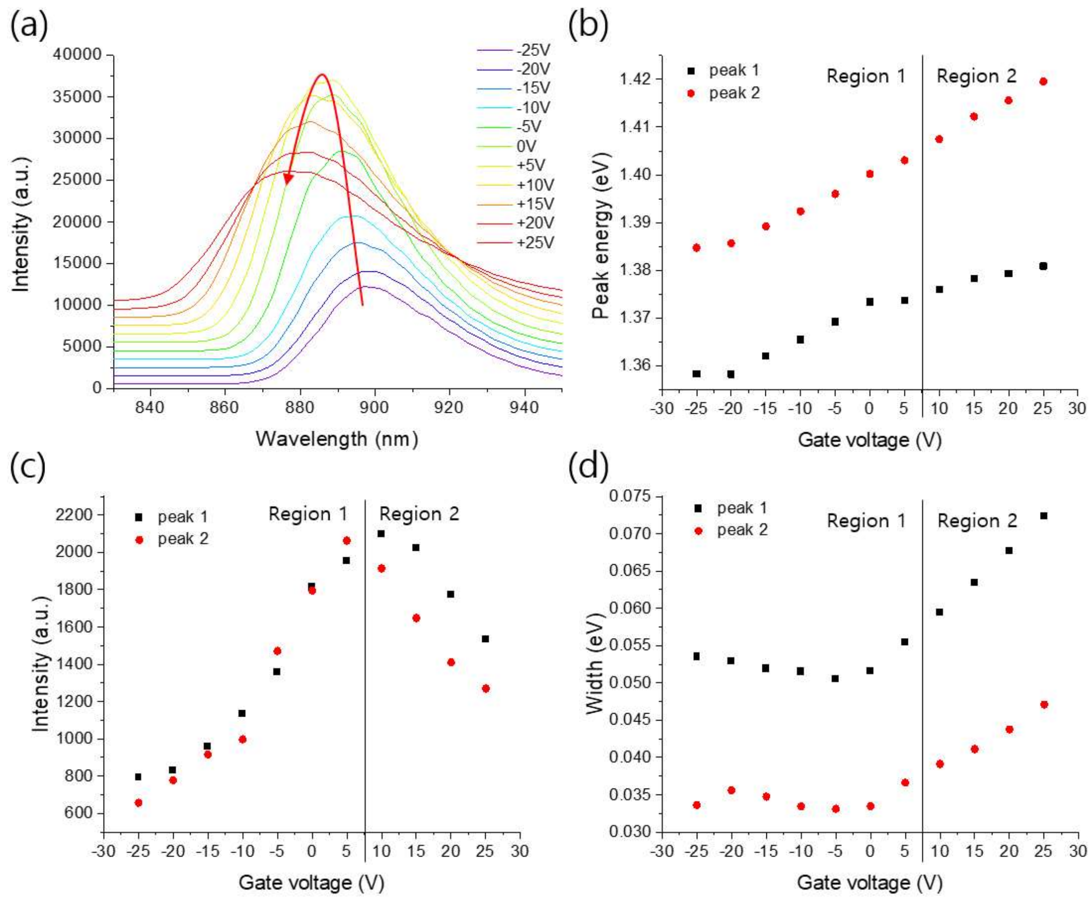

Figure 5.3 Six-layer InSe photoluminescence measurement. **(a)** Raw data, **(b)** peak energy, **(c)** intensity, and **(d)** width. Peak 1 and peak 2 correspond to defect-assisted recombination and direct electron-hole recombination, respectively.

Six-layer samples show a complex tendency while the gate voltage varies from $-25\,V$ to $+25\,V$. First of all, the voltage region is divided into two based on a point of change in intensity tendency. Region 1 corresponds to the mild hole-doping regime and region 2 corresponds to the mild electron-doping regime.

Since the intensity decreases as gate voltage moves away from the charge neutral point, exciton recombination is reduced in both regions as carrier density increases. We assume that this is accompanied with increasing trion recombinations by the non-radiative processes for both the positive trions and the negative trions. To explain region 1's redshift in energy with decreasing gate voltage from the charge neutral point, we can take into account the Pauli blocking effect. Since the six-layer has the flattest valence band among all thicknesses, small hole concentration cannot have a notable energy shift by the Pauli blocking effect. As a result, although the screening effect plays almost the same role as the electron doping regime, Pauli blocking makes almost zero blue shift. Therefore, while hole concentration increase, the overall red shift occurs due to the influence of the reduced blue shift from the Pauli blocking effect.

Region 2 corresponds to the mild electron doping regime. Since the conduction band of six-layer γ-phase InSe is not flat, the mild electron doping can make notable energy shift by Pauli blocking effect compared to the mild hole doping regime. Consequently, similar to the tendency of trilayer sample, decreasing intensity,

increasing energy, and increasing width are observed as the gate voltage increases.

Lastly, the width increases with different increasing rates in both regimes as doping level increases. Since elastic Coulomb scattering occurs with excessive charges and quasi-particles such as exciton or trion, low hole mobility means low scattering rate. This results in smaller increase rates in region 1. Due to the large difference in the mobility values which is proportional to the scattering rate, the tendency-changing point shifts slightly to the left compared to boundary between regions.

5.1.4 Discussion on the layer number dependence

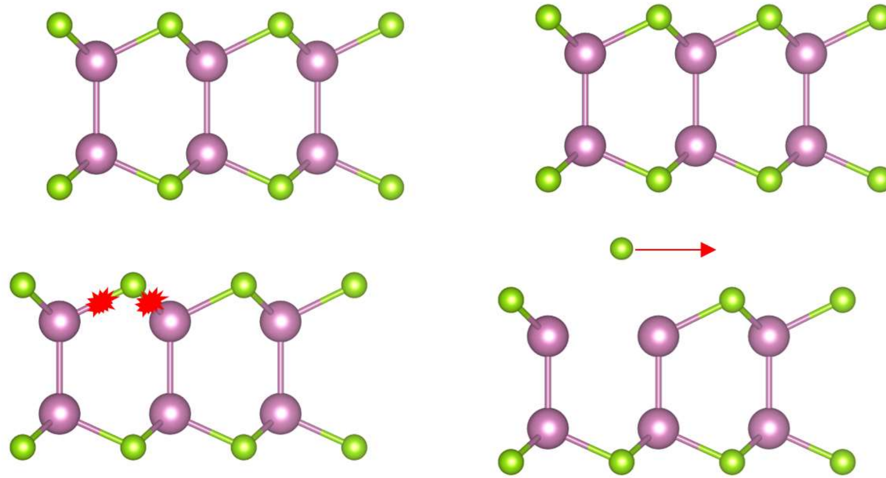

Figure 5.4 Schematic figure of defect generation in the few-layer γ-phase InSe. Se vacancies act as donors, which results in electron doping.

The remaining question about the doping dependence of photoluminescence measurement is 'why the intrinsic doping state is different as layer number changes?'. Previous work about layer-number dependent intrinsic doping state demonstrated that some Se-compounds showed the lower atomic fraction of Se as layer number decreases [32]. Theoretical calculation showed lower formation energy of Se in the thin layer limit. So, in the fabrication process, Se vacancy can be created more easily in the thin layer. These vacancies act as donor states and induce electron doping. Combined with mild

hole doping of bulk crystal, channel InSe can show both types of intrinsic electron-doped and hole-doped states depending on its thickness.

5.2 Preliminary data on spin measurement

The spin current which is large enough to be detected by optical measurement can be useful in various ways in 2D spintronics. With large spin splitting and high mobility, the spin texture can be very high in γ-phase InSe. After identifying good optical response by photoluminescence measurement, MOKE measurement was conducted.

The measured channel InSe consists of three-layer region and four-layer region for MOKE detection. The probe laser was a diode laser with a center wavelength of 741.2 nm and power of 40 μW. All measurement was conducted at 5.6 K and in vacuum environment.

Since high reference frequency of applied AC bias voltage induces large displacement current, a low reference frequency is necessary to detect electrical properties when bias current level is low. However, too low frequencies are not well-locked into lock-in amplifiers (SR830). So, the proper reference frequency is crucial for MOKE measurement with FETs. The optimized reference frequency for this MOKE measurement was 1.993 kHz.

Because InSe has high electron mobility, positive gate voltage was applied. This induces two effects. First, It allows a large amount of current to flow compared to zero gate voltage. This induces high order of spin texture. Second, as noted in the photoluminescence part, electron doping induce a blue shift in photoluminescence energy

which is advantageous for visible range laser source.

5.2.1 Spatial scan with zero bias voltage

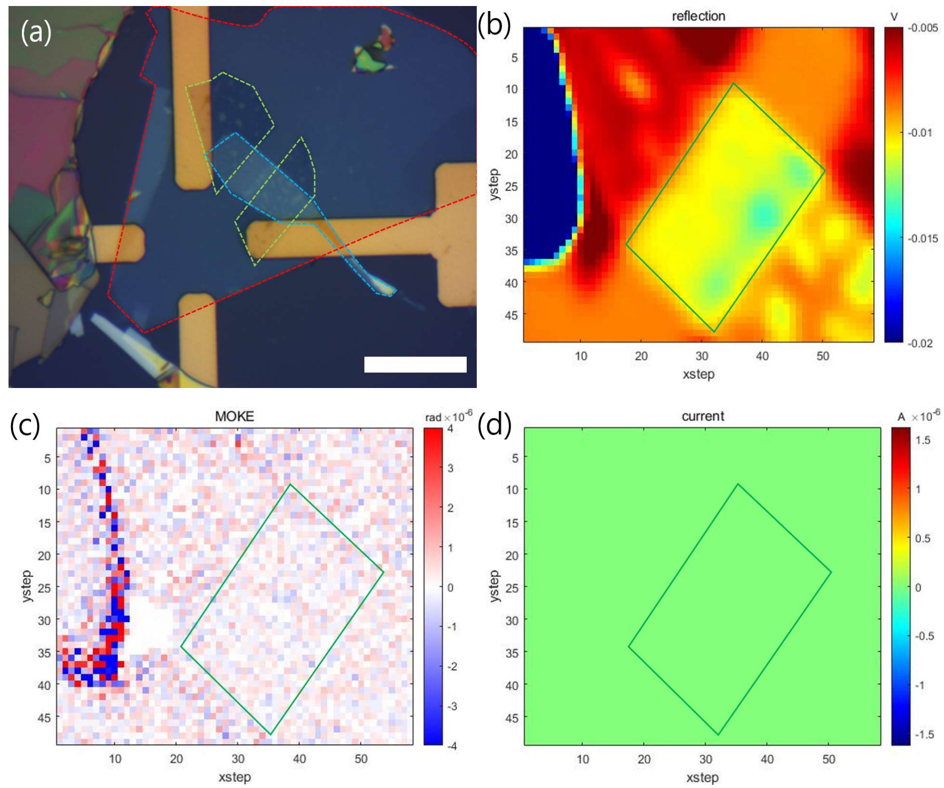

Figure 5.5 (a) Optical image of the InSe sample. Blue, green, and red dotted line corresponds to InSe, graphene, and capping hBN, respectively. The white scale bar corresponds to $15\mu m$. Spatial scan image of **(b)** reflection, **(c)** MOKE, and **(d)** current with zero bias voltage and $V_g = +20\,V$. Channel regions are indicated by green squares. The spin texture does not emerge when the bias current is zero.

After optimizing laser wavelength and reference frequency, the spatial scan was conducted for the channel region. With zero bias AC voltage and $V_g = +20\,V$, no current flows and no spin texture were observed.

5.2.2 Spatial scan with non-zero bias voltage

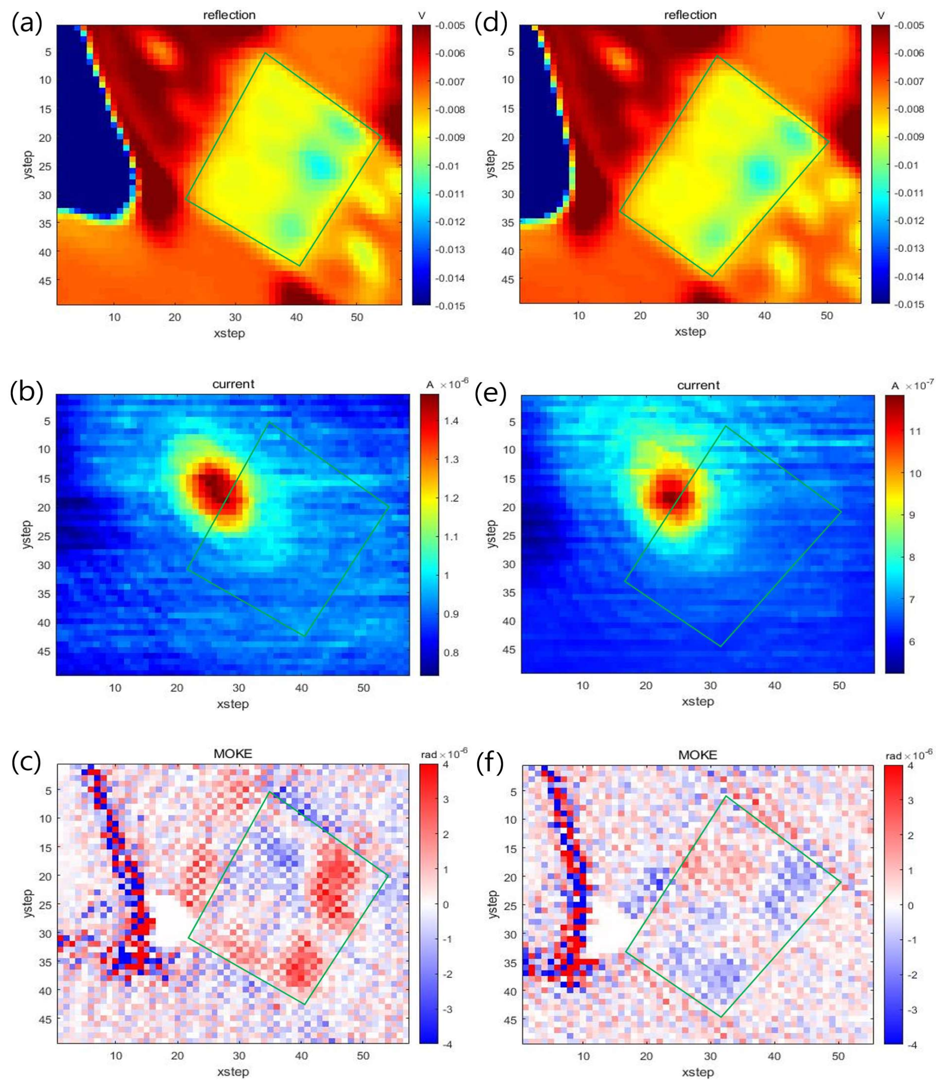

Figure 5.6 Spatial scan image of **(a)** reflection, **(b)** current, and **(c)** MOKE with $V_b = +5\,V$ and $V_g = +20\,V$. Spatial scan image of **(d)** reflection, **(e)** current, and **(f)** MOKE with $V_b = -5\,V$ and $V_g = +20\,V$. Channel regions are indicated by green squares.

To measure the current-induced spin polarization induced by bias current, the spatial scan with $V_b = +5\,V$ and $V_g = +20\,V$ was subsequently conducted. The corresponding figures are Figure 5.6 (a), (b), and (c). The channel region is identified by the reflection scan image. The bias current shows localized maximum value at the graphene/InSe interface which could be due to high photocurrent generation at that point. The maximum current is $1.5\,\mu A$. The MOKE spatial scan image shows notable regions of spin texture compared to the $V_b = 0\,V$ and $V_g = +20\,V$ case. The reason why it does not show apparent pattern is expected to be due to cracks and bubbles emerging during the fabrication process.

To verify whether the optically detected spin texture was indeed induced by the applied bias field, this result was double-checked by performing the same measurement under $V_b = -5\,V$ and $V_g = +20\,V$. The corresponding figures are Figure 5.6 (d), (e), and (f). Similar to the positive bias case, photo-current shows localized maximum value at the graphene/InSe interface. The maximum current is $1.2\,\mu A$. The MOKE spatial scan image shows the opposite sign of spin texture in the same region compared to the $V_b = +5\,V$ and $V_g = +20\,V$ case. From this data, the spin texture was double-checked to be induced by external bias, showing the possible current-induced spin polarization in few-layer InSe.

A chessboard-like pattern was found in the MOKE 2D scan, which

was caused by vibration during measurement. Although the signal-to-noise ratio is low, the measured spatial MOKE map is from the current-induced spin polarization because the overall same spin polarization pattern has been reproduced in the channel area over multiple measurements with various bias and gate voltages.

Chapter 6
Conclusion and future work

In this thesis, with various thickness of γ-phase InSe field-effect transistors, the doping dependence of photoluminescence signal, spin texture, and enhancement of channel conductivity originating from substrate dielectric screening effect are reported.

The increased dielectric screening effect by utilizing HfO_2 as a substrate enhances the bias current by about 4 times. By using HfO_2 as a high-K substrate compared to SiO_2, lower density of charge trapping states, smaller spatial range of Coulomb potentials of charge defects inside the channel InSe, and higher the atomic flatness can be achieved. All of these effects are combined to enhance the current level of the channel.

The doping dependence of photoluminescence could be well-explained by many-body effects and the high density of Se defects in the 2D limit. By analyzing the tendency of photoluminescence data, the exotic Mexican hat shape of valence band and the resulting very low hole mobility can be identified.

Lastly, the spin texture is optically observed by hand-made

magneto-optical Kerr effect (MOKE) spectroscopy. The optically detectable spin texture in InSe was first observed in this work which was verified by various measurements to exclude other possibilities.

To explain these findings firmly, more research should be done afterward. The transmission electron microscope experiment on various thicknesses of InSe and time-resolved photoluminescence measurement should be conducted to confirm the intrinsic doping difference and non-radiative trion recombinations, respectively. Also, the optimization of HfO_2 devices are expected to give higher signal of spin texture.

For future prospects, the direct observation of the spin texture by optical measurement will provide a promising route for 2D spintronics application. Doping dependence of PL emission is expected to give a new perspective on the study of TMM materials that have exotic band structures.

References

1. Novoselov, K. S. *et al.* Electric field-effect in Atomically Thin Carbon Films. *Science* **306**, 666–669 (2004).

2. Zhang, Y., Tan, Y.-W., Stormer, H. L. & Kim, P. Experimental observation of the quantum Hall effect and Berry's phase in graphene. *Nature* **438**, 201–204 (2005).

3. Novoselov, K. S. *et al.* Two-dimensional gas of massless Dirac fermions in graphene. *Nature* **438**, 197–200 (2005).

4. Mak, K. F., Lee, C., Hone, J., Shan, J. & Heinz, T. F. Atomically Thin MoS_2: A New Direct-Gap Semiconductor. *Phys. Rev. Lett.* **105**, 136805 (2010).

5. Zhao, W. *et al.* Evolution of Electronic Structure in Atomically Thin Sheets of WS_2 and WSe_2. *ACS Nano* **7**, 791–797 (2013).

6. Mak, K. F., He, K., Shan, J. & Heinz, T. F. Control of valley polarization in monolayer MoS_2 by optical helicity. *Nat. Nanotechnol.* **7**, 494–498 (2012).

7. Mak, K. F., McGill, K. L., Park, J. & McEuen, P. L. The valley Hall effect in MoS_2 transistors. *Science* **344**, 1489–1492 (2014).

8. Lee, J., Mak, K. F. & Shan, J. Electrical control of the valley Hall effect in bilayer MoS_2 transistors. *Nat. Nanotechnol.* **11**, 421–425 (2016).

9. Xiao, D., Liu, G.-B., Feng, W., Xu, X. & Yao, W. Coupled Spin and Valley Physics in Monolayers of MoS_2 and Other Group-VI Dichalcogenides. *Phys. Rev. Lett.* **108**, 196802 (2012).

10. Geim, A. K. & Grigorieva, I. V. Van der Waals heterostructures. *Nature* **499**, 419–425 (2013).

11. Radisavljevic, B., Radenovic, A., Brivio, J., Giacometti, V. & Kis, A. Single-layer MoS_2 transistors. *Nat. Nanotechnol.* **6**, 147–150 (2011).

12. Fuhrer, M. S. & Hone, J. Measurement of mobility in dual-gated MoS_2 transistors. *Nat. Nanotechnol.* **8**, 146–147 (2013).

13. Watanabe, K., Taniguchi, T. & Kanda, H. Direct-bandgap properties and evidence for ultraviolet lasing of hexagonal boron nitride single crystal. *Nat. Mater.* **3**, 404–409 (2004).

14. Wells, S. A. *et al.* Suppressing Ambient Degradation of Exfoliated InSe Nanosheet Devices via Seeded Atomic Layer Deposition Encapsulation. *Nano Lett.* **18**, 7876–7882 (2018).

15. Bandurin, D. A. *et al.* High electron mobility, quantum Hall effect and anomalous optical response in atomically thin InSe. *Nat. Nanotechnol.* **12**, 223–227 (2017).

16. Yu, Y.-J. *et al.* Tuning the Graphene Work Function by Electric field-effect. *Nano Lett.* **9**, 3430–3434 (2009).

17. Brotons-Gisbert, M. *et al.* Out-of-plane orientation of luminescent excitons in two-dimensional indium selenide. *Nat. Commun.* **10**, 3913 (2019).

18. Mudd, G. W. *et al.* The direct-to-indirect band gap crossover in two-dimensional van der Waals Indium Selenide crystals. *Sci. Rep.* **6**, 39619 (2016).

19. Magorrian, S. J., Zólyomi, V. & Fal'ko, V. I. Electronic and optical properties of two-dimensional InSe from a DFT-parametrized tight-binding model. *Phys. Rev. B* **94**, 245431 (2016).

20. Rybkovskiy, D. V., Osadchy, A. V. & Obraztsova, E. D. Transition from parabolic to ring-shaped valence band maximum in few-layer GaS, GaSe, and InSe. *Phys. Rev. B* **90**, 235302 (2014).

21. Farooq, M. U., Xian, L. & Huang, L. Spin Hall effect in two-dimensional InSe: Interplay between Rashba and Dresselhaus spin-orbit couplings. *Phys. Rev. B* **105**, 245405 (2022).

22. Chernikov, A. *et al.* Electrical Tuning of Exciton Binding Energies in Monolayer WS_2. *Phys. Rev. Lett.* **115**, 126802 (2015).

23. Gao, S., Liang, Y., Spataru, C. D. & Yang, L. Dynamical Excitonic Effects in Doped Two-Dimensional Semiconductors. *Nano Lett.* **16**, 5568–5573 (2016).

24. Zhang, Z. *et al.* Direct Observation of Band Gap Renormalization in Layered Indium Selenide. *ACS Nano* **13**, 13486–13491 (2019).

25. Plechinger, G. *et al.* Identification of excitons, trions and biexcitons in single-layer WS_2. *Phys. Status Solidi RRL - Rapid Res. Lett.* **9**, 457–461 (2015).

26. Iwata, Y., Banal, R. G., Ichikawa, S., Funato, M. & Kawakami, Y. Emission mechanisms in Al-rich AlGaN/AlN quantum wells assessed by excitation power dependent photoluminescence spectroscopy. *J. Appl. Phys.* **117**, 075701 (2015).

27. Mudd, G. W. *et al.* Quantum confined acceptors and donors in InSe nanosheets. *Appl. Phys. Lett.* **105**, 221909 (2014).

28. Dolui, K., Rungger, I. & Sanvito, S. Origin of the n-type and p-type conductivity of MoS_2 monolayers on a SiO_2 substrate. *Phys. Rev. B* **87**, 165402 (2013).

29. Zhan, Y., Liu, Z., Najmaei, S., Ajayan, P. M. & Lou, J. Large-Area Vapor-Phase Growth and Characterization of MoS_2 Atomic Layers on a SiO_2 Substrate. *Small* **8**, 966–971 (2012).

30. Ma, N. & Jena, D. Charge Scattering and Mobility in Atomically Thin Semiconductors. *Phys. Rev. X* **4**, 011043 (2014).

31. Venanzi, T. *et al.* Photoluminescence dynamics in few-layer InSe. *Phys. Rev. Mater.* **4**, 044001 (2020).

32. Wang, Z. *et al.* Controllable Doping in 2D Layered Materials. *Adv. Mater.* **33**, 2104942 (2021).

Abstract in Korean

최근 전이금속 모노칼코게나이드(TMM)가 흥미로운 2차원 반도체로 떠오르고 있다. 특히, InSe는 6층 두께에서 direct-to-indirect 밴드갭 전이와 함께 물질 층수에 강하게 의존하는 밴드 구조를 가지고 있다. 이것은 특이한 광학 및 전기적 특징을 유도하며 최근 활발히 연구되고 있다. 또한 gating으로 인한 외부 도핑 및 고유 스핀 분할을 활용하면 도핑 의존성 엑시톤 방출의 특이한 성질 및 전자 스핀 텍스처를 측정할 가능성이 있다. 본 논문에서는 few-layer InSe field-effect transistors (FETs)를 제작하고 광발광 분광법과 자기광학 커 효과 분광법으로 InSe의 광학 및 전기적 특징의 도핑 의존성을 측정하였다.